Coulomb Blockade in a Coupled Nanomechanical Electron Shuttle

Chulki Kim,[†] Marta Prada,[†,‡] and Robert H. Blick[†,§,*]

[†]Department of Physics and [§]Department of Electrical and Computer Engineering, University of Wisconsin-Madison, Madison, Wisconsin 53706, United States, and [‡]ICMM-CSIC, Sor Juana Ines de la Cruz, 3, 28049 Madrid, Spain

ABSTRACT We demonstrate single electron shuttling through two coupled nanomechanical pendula. The pendula are realized as nanopillars etched out of the semiconductor substrate. Coulomb blockade is found at room temperature, allowing metrological applications. By controlling the mechanical shuttling frequency we are able to validate the different regimes of electron shuttling.

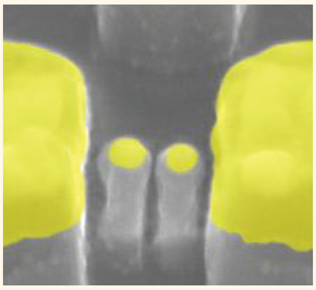

KEYWORDS: Coulomb blockade · electron shuttling · nanopillars · coupled pendula

One of the fundamental experiments in classical mechanics is the coupled pendula, used to demonstrate how energy is transferred from one resonator to another. This coupled pendula or coupled oscillator model is often evoked as an analogy for the Josephson effect in superconducting junctions, where similar differential equations can be applied.[1] In principle, the physics of coupled oscillators can be found in mode-locked lasers,[2] analyzing weather fronts in climate modeling,[3] and neural networks.[4]

Nanotechnology delivers the tools to fabricate nanoscale electro-mechanical systems, pushing toward the ultimate limits of miniaturization.[5−9] This has already led to the realization of single nanomechanical pendula in various forms, for example, suspended semiconductor cantilevers[10−12] and nanopillars.[13−15] Such a mechanical resonator is commonly placed between two electrodes, so that the pendulum can exchange electrons and mechanically transfer them from source to drain. Hence, the term electron shuttle was coined.[16,17] Here we present measurements of two coupled pendula realized as nanopillars integrated between two contacts. The strongly reduced cotunneling in two serially coupled electron shuttles reveals Coulomb blockade (CB) at room temperature. The fundamental importance of CB in nanomechanical shuttles is 2-fold: one in metrology application as outlined by Weiss and Zwerger[18] and the second in ultrasensitive nanomechanical sensors.

In classical electron turnstiles,[19] the stochastic nature of tunneling is typically suppressed by operating the turnstile at frequencies f, much lower than the inverse of the time constant τ (or, more formally, the $1/\tau = 1/RC$-frequency of the contacts). In contrast to this, we are able to operate electron shuttles in the regime of high-frequencies (*i.e.*, $f \approx \tau^{-1}$), and show that the clocking of electron transport can be achieved. This effect is due to the suppression of cotunneling when the shuttles are operated in series.[18] The two shuttles considered here are placed between two nanoscale contacts. We characterize the device's response by probing the direct current through the nanopillars. Mechanical motion is studied first by coupling a DC-bias and then, exciting the mechanical motion by adding a radio frequency (RF) signal to the source electrode, as we have demonstrated before.[20]

The two nanopillars are defined on a silicon-on-insulator (SOI) substrate, where the top crystalline silicon is 190 nm thin and the insulating SiO_2 is about 350 nm. A 50 nm top gold layer serves as the final electrical conduction path. The deposited metal is also employed as a mask in a dry etch step, which mills out the SOI material around the pillars. We apply a CF_4 plasma etch step and mill into the SiO_2 insulating layer, thus ensuring electron transport *via* the metallic islands. Further details on the processing are given by Kim *et al.*[14] In Figure 1a, the final sample is shown in a scanning electron microscope graph. The source and drain contacts are placed in close proximity to the two pillars. The distance between the pillars is about 17 nm. The gating electrode is placed further away, enabling a shift in the electrostatic potential of the islands. The inset of Figure 1a gives a broader view of the coplanar-waveguides into which the two nanopillars are embedded.

* Address correspondence to blick@engr.wisc.edu.

Received for review October 26, 2011 and accepted December 27, 2011.

10.1021/nn204103m

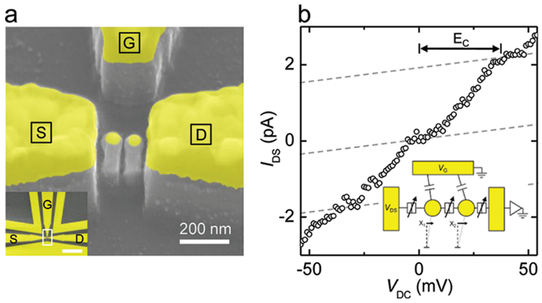

Figure 1. (a) Two coupled electron shuttles realized as nanopillars. The metallic top layer allows electron exchange with the source (*S*) and drain (*D*) contacts. The scale bar corresponds to a length of 200 nm. The inset shows a broader view of the coplanar-waveguide into which the nanopillars are embedded. The scale bar in the inset is 10 μm. (b) DC response: The dashed lines indicate the Coulomb staircase. The nonzero slope of the staircase steps is due to thermal broadening. The inset gives the circuit diagram with the mechanically tunable tunneling barriers coupling the leads and shuttles. The gate couples capacitively with the two electron islands.

The nanoscale circuit is placed in an impedance matched transmission line in order to minimize signal loss along the line. All measurements are performed under vacuum (<10^{-5} mbar) in a probe station at room temperature. The station is placed in a Faraday cage and equipped with radio frequency contact probes covering the range from DC to 50 GHz (a bias-tee allows AC/DC superposition with high precision). The equivalent circuit diagram is given in the inset of Figure 1b: The two pillars are individually displaced by x_1 and x_2, which lead to tunable resistances and mutual capacitances (arrow boxes). The gating electrode couples capacitively to the pillars. The output current of the coupled electron shuttles is fed into a current amplifier.

RESULTS AND DISCUSSION

The resulting *IV*-characteristic is shown in Figure 1b: the application of a DC bias voltage only across the coupled pendula leads to an ohmic response, modulated by Coulomb blockade steps. The gate electrode is grounded in these measurements. The total Coulomb energy E_C marks the energy required to transport a single charge through an island.[21] From the data in Figure 1b (marked by the arrow) we find a total energy of $E_C \approx 40$ meV. The capacitance of each island of radius r_{np} can be estimated to be $C_{np} \simeq 4\pi\varepsilon_0 r_{np}(1 + (r_{np}/d)^2)$, where the internanopillar distance is d = 80 nm. In accordance with the optimized values that fit the experimental model (see Methods section), we obtain $C_{np1} \simeq 3.2$ aF and $C_{np2} \simeq 3.9$ aF, where we used for the islands' radii the values $r_{np1} = 25$ nm and $r_{np2} = 31$ nm. Since the two islands are placed in series, the total capacitance is $C^{-1} \approx C_{np1}^{-1} + C_{np2}^{-1}$. Hence, we obtain a total capacitance of $C \approx 1.76$ aF, from which we extract a Coulomb energy of $E_C = e^2/2C = 41$ meV. This is well above the corresponding room temperature energy of 26 meV. We stress that room temperature CB for a coupled shuttle has not been observed before. Conventional single electron shuttles reveal CB only at low temperature,[22,23] since suppression of cotunneling is not as pronounced as for the coupled shuttles considered in this work.

In Figure 2 the response to a pure DC-bias V_{DC} and gate voltage V_G of the coupled shuttles is studied. *IV*-curves at altered gate voltages are shown in Figure 2(a–c). The dashed lines are linear extrapolations of the initial conductance slopes and underline the steps caused by single electron charging. Evidently, a typical Coulomb staircase is superimposed on an ohmic response, due to thermal broadening and shuttling.[16] Note that the mechanical motion of the shuttles allow exchange of electrons with one electrode while suppressing it on other electrode. Since the applied gate voltage changes the potential around the shuttles, the charging energy required for an additional electron on the island can be varied accordingly. The trace at V_G = 25 mV in Figure 2b shows an ohmic response without the CB steps. As the gate voltage decreases, the Coulomb staircase reappears ($V_G = -55$ mV), as shown in Figure 2c. The traces are not symmetric about zero bias, which is due to the slightly different diameters of the nanopillar islands and the possible polarization of an oxide layer on the islands.[24] The full DC output signal from a measurement run is summarized with respect to both V_G and V_{DC} in Figure 2d, revealing Coulomb diamonds. We note that the diamond structure compares to that of a single island, due to the common V_G and the similar size of the islands. The lack of symmetry of the diamonds with respect to $V_{DC} = 0$ is due to the actual difference in island radii, and to the difference in capacitance couplings to the source or drain. Although the obtained *IV* curves do not show clear steps due to the thermal environment, the periodic variation of the source-drain offset voltages is seen. The line plots for V_G = 55, 25, and -55 mV are indicated by the white horizontal lines in Figure 2d. To validate the experimental results, we compute the current using numerical methods (see the Methods section). The theoretical results shown in Figure 2e reproduce the shape and size of the measured Coulomb diamonds and agree with the estimated size of the islands.

Next we apply an RF signal with zero DC bias in order to tune the mechanical motion of the system, as shown in Figure 3a. The ability to "dial in" the shuttling frequency is the fundamentally new feature of this device, as compared to classical single electron transistors. We can now trace the DC bias voltages at the three different mechanical modes marked in Figure 3a, plotted in Figure 3 panels b, c, and d, respectively. These correspond to commensurate mode numbers *p*/*q* of the fundamental mode (for more details, see ref 20): *p*/*q* is 1/6 (circle, *f* = 87 MHz), 5/9 (square, *f* = 289 MHz) and 1/1 (triangle, *f* = 500 MHz). The current offset I_{SB} due to spontaneous symmetry breaking (SB) in coupled electron

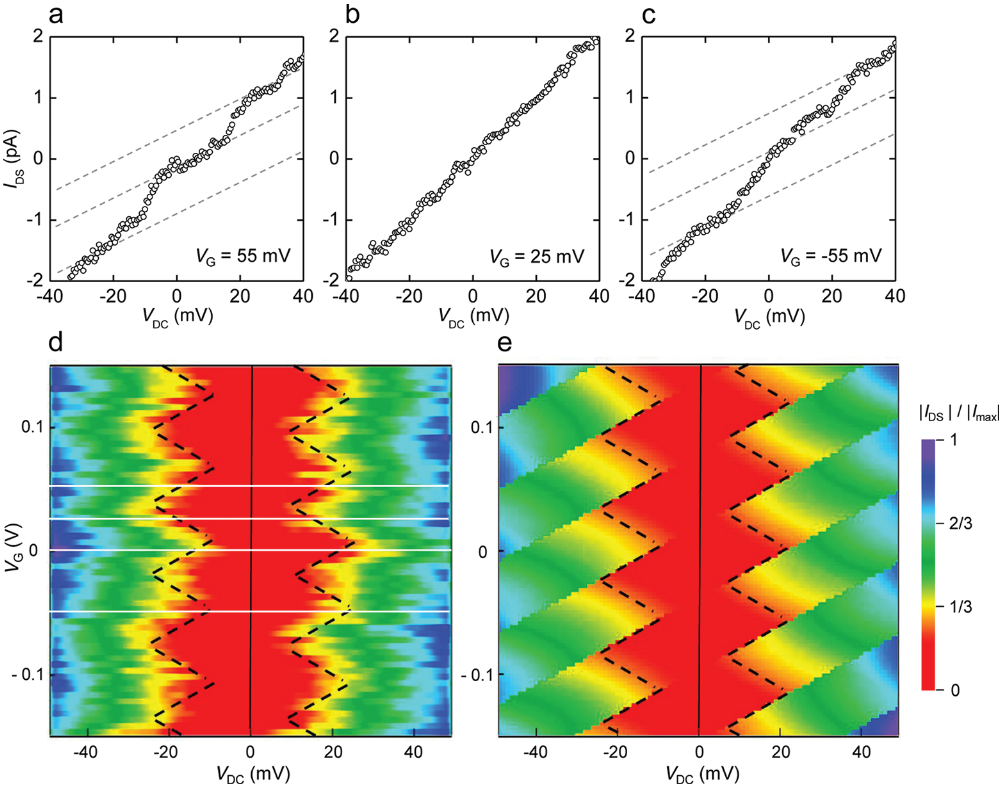

Figure 2. Coulomb blockade in the coupled electron shuttle: (a−c) Current I_{DS} traces *vs* bias voltage V_{DC} for gate voltages 55, 25, and −55 mV. Experimental (d) and theoretical (e) Coulomb diamonds traced in the normalized current, $|I_{DS}|/I_{DS}^{max}$, in color scale representation. The lower borders of the CB regions are represented in red with the Coulomb plateaus depicted in green (see color scale). The borders of the CB determined from the theory plots are marked by dashed black lines as a guide to the eye, both in panels d and e. The theoretically derived lines trace the measurements closely. The horizontal lines in panel d indicate the previously shown line plots in Figure 1b and Figure 2(a−c).

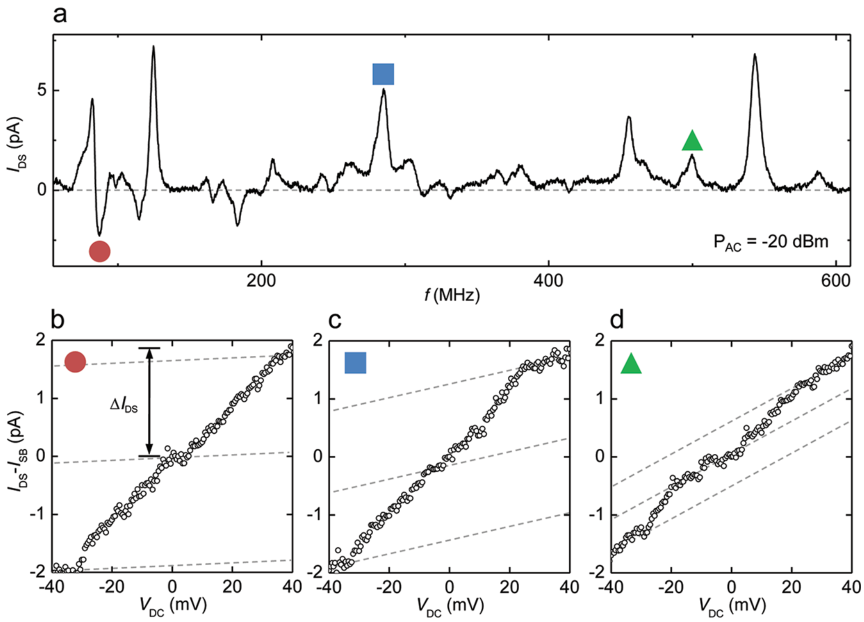

Figure 3. (a) Full frequency sweep of the direct current (I_{DS}) through the coupled shuttle revealing the mechanical mode structure for V_{DC} = 0. The colored symbols indicate three distinct mechanical frequencies plotted in (b−d). The lower traces indicate the DC signal at those different modes: *f* = 87, 285, and 500 MHz, respectively.

shuttles[20] is subtracted. Dashed lines extend the inclined plateaus to underline the staircase current.

Figure 4a exemplifies the dissipative regime: In this limit, a saturation current (frequency independent) is

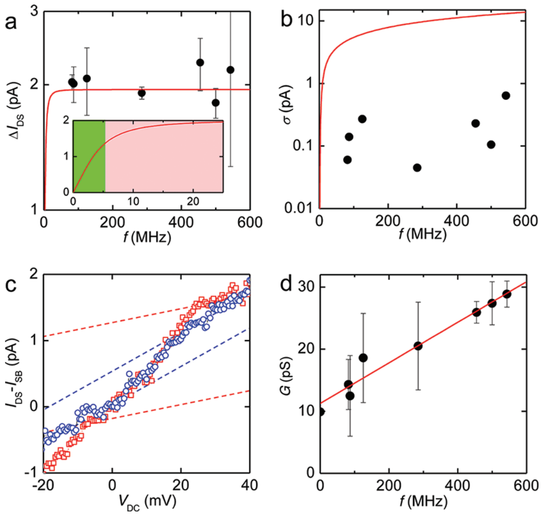

Figure 4. Evaluation of time dependent shuttling: (a) The current steps between plateaus ΔI_{DS} are plotted *vs* the mechanical frequency *f* at a fixed gate voltage ($V_G = 0$ V). The measured current steps (black dots) fall on the expected flat-line, as predicted.[18] The inset shows a theoretical plot of the expected current in the low frequency region. The coupled shuttles are operated above the cutoff frequency τ^{-1} (red region). (b) The standard deviation σ of the measured current (black dots). This is compared to the theoretical expression for charge fluctuation in a single shuttle (red solid line) as obtained from ref 18. The strongly reduced cotunneling leads to a suppression of fluctuations, allowing the observation of CB. (c) *IV*-traces for two mechanical modes, as seen the slopes in the plateau increase from a shuttling frequency of 285 MHz (red squares) to 500 MHz (blue circles). (d) Summary of the differential conductance within the Coulomb-plateau for the different shuttling modes. As expected the effective differential conductance is increased due to the mechanically enhanced escape rate of the electrons.

achieved, as the effective contact time of the islands with the electrodes is proportional to the inverse of the frequency, and at the same time, the current is proportional to the contact time and to the frequency (see Methods section). We observe a saturation value for the current of about 2 pA. The measured current steps (black dots) fall on the expected shuttle current (red solid line), as predicted from eq 2. We have to note that their calculation only considered a single shuttle. The inset in Figure 4a shows a magnified view of the expected current in the low frequency region. The coupled shuttles are operated in the high frequency, dissipative limit (red region). We estimated $x_{max} \approx 5-8$ nm, $d \approx 17$ nm, and $\lambda \approx 1$ nm, giving $t_0 \approx 1/(2\omega)$. We also have $\tau \approx \times 10^{-7}$ s. Thus, we find the transition frequency to be of the order of 5 MHz, which agrees very well with our data. The standard deviation σ of the experimental values are found to be much lower than the theoretically expected fluctuations, as seen in Figure 4b. This can be ascribed to the fact that the model assumed a single shuttle unlike the actual device of two coupled charge shuttles in series. However, charge fluctuations are even more strongly suppressed by the mechanical resonances for two coupled shuttles.

We consider now the conductance level within the plateau. Figure 4c shows two *IV*-traces at 285 MHz (red squares) and 500 MHz (blue circles). The dashed lines give the slopes of the corresponding plateaus in the neighboring Coulomb regions. The slope, or differential conductance $G = \Delta I_{DS}/\Delta V_{DC}$, increases linearly toward higher shuttling frequencies, a consequence of self-excitation. This occurs around $V_{DC} = 0$, where a mechanical mode was located, and at $V_{DC} > V_c$. In the CB regime, the number of transferred electrons per period is quantized in units of *e*, $Ne \propto (V_{DC}C/e + {}^1/_2)e$. Moreover, in the self-oscillatory regime (above a critical voltage, V_c,[16] or around $V_{DC} = 0$, where the mechanical mode was excited), the charge exchange with the leads takes a fixed quantized value corresponding to the thermal equilibrium with the nearest lead, and is exponentially suppressed with the far lead. Following Gorelik *et al.* we estimate the critical voltage V_c to be of the order of the CB voltage, $V_c \approx e/C$.[16] In this regime, the conventional linear-in-frequency relation applies, $I \simeq 2Nef$. Note that for intermediate V_{DC} values, $0 < V_{DC} < V_c$, the amplitude of the self-oscillations is suppressed. In this region, eq 2 applies, rather than the linear-in-frequency relation (see also the Methods section). The overall results are summarized in Figure 4d, where we show the step differential conductance in the plateau, $\Delta I_{DS}/\Delta V_{DC}$, or the slope of the dashed lines of Figure 4c. The linearity in frequency of the plateau differential conductance *G* is evident. This demonstrates the self-excitation of the nanopillars, already shown to cause ohmic behavior.[15,27]

CONCLUSION

In summary we observe Coulomb blockade in a coupled electron shuttle operating at room temperature. Mechanical clocking of electron transport has been demonstrated by using RF signals. Operating in the high frequency regime leads to a strong suppression of current fluctuations. Two regimes of operation are observed in the high frequency limit as a function of bias voltage, corroborating theoretical predictions: the dissipative regime, where the current is frequency independent, and the self-oscillatory CB regime, showing a linear-in-frequency conductance.

METHODS

To validate the experimental results obtained in Figure 2a–d, we compute the current within the orthodox model of CB. The accessible states are described by their respective probabilities P_{n_1,n_2}, where n_i is the number of excess electrons on the islands $i = 1,2$. In the absence of an RF signal, the system can be assumed to be in the dissipative regime, where the amplitude of the mechanical oscillations is small and the tunneling current prevails over the shuttle current.[16] Changes in the resistance of a particular junction are proportional to $e^{x_i/\lambda}$, with λ being the typical tunneling distance, x_i the displacement, and $x_i \lesssim \lambda$ in the dissipative regime. In this limit, we suppose $1/\Gamma$ to be much smaller than the typical time scale of the displacements, and the time evolution can be described in terms of coupled master equations,[25] which we solve by exact diagonalization. In the CB limit, we observe that $\langle|I_{DS}|\rangle/I_{DS}^{max} \propto \Sigma_{n_1,n_2} P_{n_1,n_2}(\vec{\Gamma}_{n_1,n_2} - \overleftarrow{\Gamma}_{n_1,n_2})$, where $\langle ... \rangle$ denotes an ensemble average. $\vec{\Gamma}_{n_1,n_2}$ gives the rate of tunneling from left to right at one of the junctions for a given configuration $\{n_1,n_2\}$:

$$\vec{\Gamma}_{n_1,n_2} = \left(\frac{1}{e^2R}\right)\frac{\Delta E(n_1,n_2)}{\exp[\Delta E(n_1,n_2)/k_B T] - 1} \qquad (1)$$

where R is the average resistance of the junction and ΔE is the chemical potential. The theoretical results are shown in Figure 2e: the CB region below the first transition is shown in red. We stress that a finite conductance is observed in this region due to thermal broadening and direct electron shuttling. In the dissipative regime, however, we assume temperature broadening to be the dominant source of the ohmic response.

We now focus on the ohmic response between the differential conductance plateau or current step, ΔI_{DS}. Conventionally, one would expect a simple linear relation between this ohmic current and the shuttling frequency of the form, $I = 2ef$ or $\Delta I_{DS} \approx f$, which is typically applied for electrometry purposes.[26] This relation, however, is only valid in the limit of large tunneling rates, $\vec{\Gamma}_{i,j} \gg f^{-1}$ with $\vec{\Gamma}_{i,j}$ defined in eq 1. For our setup, the relation applies only in the self-oscillatory regime, achieved in the plateau or around $V_{DC} = 0$, where a mechanical mode is excited. Our theoretical results indicate that in the interplateau region $\Gamma_{i,j} \lesssim 5-15$ MHz, which is slower than the mechanical motion. Hence, we can state that the coupled shuttles operate in the dissipative regime. According to Weiss and Zwerger,[18] we can calculate in this regime the average number of transferred electrons $\langle N \rangle$ per period:

$$\langle N \rangle = \frac{2(1 - a^3)}{(1+a)(1+1/2a+a^2)} \qquad (2)$$

where $a \equiv \exp(-t_0/\tau)$, and $2t_0$ is the effective contact time, $t_0 \equiv \omega^{-1}(\pi\lambda/(2x_{max}))^{1/2}(1 + (\lambda/(2d))$. The length x_{max} indicates the maximum displacement of the mechanical oscillation, and $\omega = 2\pi f$. In the regime of high RF, the effective contact time is shorter than the charge relaxation time, $t_0 \ll \tau$. Thus the number of transferred electrons per period is inversely proportional to the frequency of the shuttle oscillation, $\langle N \rangle \propto t_0$ with $t_0 \propto 1/f$. Then, the electron shuttle current achieves a frequency independent saturation value, $I = \langle N \rangle ef \propto \Delta I_{DS}$.

Acknowledgment. We are grateful to G. Platero for enlightening discussions. The authors thank DARPA for support through the NEMS-CMOS Program N66001-07-1-2046, the University of Wisconsin-Madison for support with a Draper-TIF award, and the Spanish Ministry of Education, Program SB2009-0071.

REFERENCES AND NOTES

1. Tinkham, M. I. *Introduction to Superconductivity*; McGraw-Hill: New York, 1996.
2. Leuzzi, L.; Conti, C.; Folli, V.; Angelani, L.; Ruocco, G. Phase Diagram and Complexity of Mode-Locked Lasers: From Order to Disorder. *Phys. Rev. Lett.* **2009**, *102*, 083901–083905.
3. Chang, P.; Yamagata, T.; Schopf, P.; Behera, S. K.; Carton, J.; Kessler, W. S.; Meyers, G.; Qu, T.; Schott, F.; Shetye, S.; Xie, S. − P.; *et al.* Climate Fluctuations of Tropical Coupled Systems—The Role of Ocean Dynamics. *J. Climate* **2006**, *19*, 5122–5174.
4. Han, K. H.; Postnov, D. E. Chaotic Bursting as Chaotic Itinerancy in Coupled Neural Oscillators. *Chaos* **2003**, *13*, 1105–1110.
5. Blick, R. H.; Erbe, A.; Pescini, L.; Kraus., A.; Scheible, D. V.; Beil, F. W.; Hoehberger, E.; Hoerner, A.; Kirschbaum, J.; Lorenz, H.; *et al.* Nanostructured Silicon for Studying Fundamental Aspects of Nanomechanics. *J. Phys. Condens. Matter* **2002**, *14*, R905–R945.
6. Blencowe, M. Nanomechanical Quantum Limits. *Science* **2004**, *304*, 56–57.
7. Roukes, M. L. Nanoelectromechanical Systems Face the Future. *Phys. World* **2001**, *14*, 25–32.
8. Craighead, H. G. Nanoelectromechanical Systems. *Science* **2000**, *290*, 1532–1535.
9. Cleland, A. N. *Foundations of Nanomechanics*; Springer: New York, 2002.
10. Erbe, A.; Weiss, C.; Zwerger, W.; Blick, R. H. Nanomechanical Resonator Shuttling Single Electrons at Radio Frequencies. *Phys. Rev. Lett.* **2001**, *87*, 096106–096109.
11. Scheible, D. V.; Weiss, C.; Kotthaus, J. P.; Blick, R. H. Periodic Field Emission from an Isolated Nanoscale Electron Island. *Phys. Rev. Lett.* **2004**, *93*, 186801–186804.
12. Koenig, D.; Weig, E. M.; Kotthaus, J. P. Ultrasonically Driven Nanomechanical Single-Electron Shuttle. *Nat. Nanotechnol.* **2008**, *3*, 482–489.
13. Scheible, D. V.; Blick, R. H. Silicon Nanopillars for Mechanical Single-Electron Transport. *Appl. Phys. Lett.* **2004**, *84*, 4632–4634.
14. Kim, H. S.; Qin, H.; Blick, R. H. Direct Mechanical Mixing in a Nanoelectromechanical Diode. *Appl. Phys. Lett.* **2007**, *91*, 143101–143103.
15. Kim, H. S.; Qin, H.; Blick, R. H. Self-Excitation of Single Nanomechanical Pillars. *New J. Phys.* **2010**, *12*, 033008–033010.
16. Gorelik, L. Y.; Isacsson, A.; Voinova, M. V.; Kasemo, B.; Shekhter, R. I.; Jonson, M. Shuttle Mechanism for Charge Transfer in Coulomb Blockade Nanostructures. *Phys. Rev. Lett.* **1998**, *80*, 4526–4529.
17. Shekhter, R. I.; Gorelik, L. Y.; Jonson, M.; Galperin, Y. M.; Vinokur, V. M. Nanomechanical Shuttle Transfer of Electrons. *J. Comput. Theor. Nanosci.* **2007**, *4*, 860–895.
18. Weiss, C.; Zwerger, W. Accuracy of a Mechanical Single-Electron Shuttle. *Europhys. Lett.* **1999**, *47*, 97–103.
19. Geerligs, L. J.; Anderegg, V. F.; Holweg, P. A. M.; Mooij, J. E. Frequency-Locked Turnstile Device for Single Electrons. *Phys. Rev. Lett.* **1990**, *64*, 2691–2694.
20. Kim, C.; Park, J.; Blick, R. H. Spontaneous Symmetry Breaking in Two Coupled Nanomechanical Electron Shuttles. *Phys. Rev. Lett.* **2010**, *105*, 067204–067207.
21. Holleitner, A. W.; Blick, R. H.; Hüttel, A. K. H.; Eberl, K.; Kotthaus, J. P. Probing and Controlling the Bonds of an Artificial Molecule. *Science* **2002**, *297*, 70–72.
22. Azuma., Y.; Hatanaka, T.; Kanehara, M.; Teranishi, T.; Chorley, S.; Prance, J.; Smith, C. G.; Majima., Y. One by One Single-Electron Transport in Nanomechanical Coulomb Blockade Shuttle. *Appl. Phys. Lett.* **2007**, *91*, 053120–053122.
23. Azuma, Y.; Kanehara, M.; Teranishi, T.; Majima, Y. Single Electron on a Nanodot in a Double-Barrier Tunneling Structure Observed by Noncontact Atomic-Force Spectroscopy. *Phys. Rev. Lett.* **2006**, *96*, 016108–016111.
24. Wilkins, R.; Ben-Jacob, E.; Jaklevic, R. C. Scanning-Tunneling-Microscope Observations of Coulomb Blockade and Oxide Polarization in Small Metal Droplets. *Phys. Rev. Lett.* **1989**, *63*, 801–803.
25. Ahn, K.-H.; Park, H. C.; Wiersig, J.; Hong, J. Current Rectification by Spontaneous Symmetry Breaking in Coupled Nanomechanical Shuttles. *Phys. Rev. Lett.* **2006**, *97*, 216804–216807.
26. Grabert, H.; Devoret, M. H. *Single Charge Tunneling: Coulomb Blockade Phenomena in Nanostructures*; Plenum: New York, 1992.
27. Weldon, J. A.; Alemán, B.; Sussman, A.; Gannett, W.; Zettl, A. K. Sustained Mechanical Self-Oscillations in Carbon Nanotubes. *Nano Lett.* **2010**, *10*, 1728–1733.